Bioorganic Chemistry 102 (2020) 104048

Contents lists available at ScienceDirect

Bioorganic Chemistry

journal homepage: www.elsevier.com/locate/bioorg

Novel *N*-substituted 5-phosphate-D-arabinonamide derivatives as strong inhibitors of phosphoglucose isomerases: Synthesis, structure-activity relationship and crystallographic studies

Lama Ahmad[a], Stéphane Plancqueel[b], Noureddine Lazar[b], Hafsa Korri-Youssoufi[a], Inès Li de la Sierra-Gallay[b], Herman van Tilbeurgh[b], Laurent Salmon[a,*]

[a] Institut de Chimie Moléculaire et des Matériaux d'Orsay (ICMMO), Equipe de Chimie Bioorganique et Bioinorganique, CNRS UMR8182, LabEx LERMIT, Université Paris-Saclay, Rue du Doyen Georges Poitou, bât. 420, 91405 Orsay Cedex, France
[b] Institut de Biologie Intégrative de la Cellule (I2BC), CNRS UMR9198, Université Paris-Saclay, Rue du Doyen Georges Poitou, bât. 430, 91405 Orsay Cedex, France

ARTICLE INFO

Keywords:
Enzyme inhibitor
Phosphate
Monosaccharide
Phosphoglucose isomerase
Autocrine motility factor

ABSTRACT

Phosphoglucose isomerase (PGI) is a cytosolic enzyme that catalyzes the reversible interconversion of D-glucose 6-phosphate and D-fructose 6-phosphate in glycolysis. Outside the cell, PGI is also known as autocrine motility factor (AMF), a cytokine secreted by a large variety of tumor cells that stimulates motility of cancer cells in vitro and metastases development in vivo. Human PGI and AMF are strictly identical proteins both in terms of sequence and 3D structure, and AMF activity is known to involve, at least in part, the enzymatic active site. Hence, with the purpose of finding new strong AMF-PGI inhibitors that could be potentially used as anticancer agents and/or as bioreceptors for carbohydrate-based electrochemical biosensors, we report in this study the synthesis and kinetic evaluation of several new human PGI inhibitors derived from the synthon 5-phospho-D-arabinono-1,4-lactone. Although not designed as high-energy intermediate analogue inhibitors of the enzyme catalyzed isomerization reaction, several of these *N*-substituted 5-phosphate-D-arabinonamide derivatives appears as new strong PGI inhibitors. For one of them, we report its crystal structure in complex with human PGI at 2.38 Å. Detailed analysis of its interactions at the active site reveals a new binding mode and shows that human PGI is relatively tolerant for modified inhibitors at the "head" C-1 part, offering promising perspectives for the future design of carbohydrate-based biosensors.

1. Introduction

Phosphoglucose isomerase (PGI, E.C. 5.3.1.9) is a cytosolic enzyme that catalyses the reversible interconversion of D-glucose 6-phosphate (G6P) and D-fructose 6-phosphate (F6P) in glycolysis. In addition to isomerase activity, PGI displays anomerase activity between anomers of D-glucopyranose 6-phosphate (α/β-G6P) [1] and between those of D-fructofuranose 6-phosphate (α/β-F6P) [2] (Scheme 1A). The F6P to G6P isomerization reaction proceeds by a proton transfer mechanism between C-1 and C-2 of the substrates, concomitant with a proton transfer between O-1 and O-2, and involves a 1,2-*cis*-enediolate high-energy intermediate (HEI). Designed as HEI analogues, 5-phospho-D-arabinonohydroxamate (5PAH, **1**) [3] and 5-phospho-D-arabinonate (5PAA, **2**) [4] are the strongest PGI inhibitors reported to date (Scheme 1B). In complement with kinetic and physico-chemical studies, a number of crystal structures of PGI, including PGI alone (human PGI: PDB code 1IAT [5], rabbit PGI: PDB code 1HM5 [6]) and in complex with substrate D-fructose 6-phosphate (rabbit PGI: PDB code 1HOX [7]) or inhibitors **1** (rabbit PGI: PDB code 1KOJ [8]), **2** (rabbit PGI: PDB code 1G98 [9], human PGI: PDB code 1NUH [10]), and D-sorbitol-6-phosphate (rabbit PGI, PDB code 1XTB [11]), led to a detailed mechanism of the overall catalyzed interconversion.

PGI is also known as a moonlighting protein [12] with a number of extracellular activities including roles as neuroleukin [13,14], differentiation and maturation mediator [15], antigen in rheumatoid arthritis [16], surface antigen in sperm agglutination [17], inhibitor toward myofibril-bound serine proteinase [18], and autocrine motility factor (AMF) [19,20]. AMF is a cytokine secreted by a large variety of tumor cells that stimulates motility of cancer cells in vitro and metastases development in vivo [21]. AMF is a validated biomarker of cancer progression [22–26], high levels of the cytokine in urine or serum of cancer patients being clearly related to poor prognosis. While

* Corresponding author.
E-mail address: laurent.salmon@universite-paris-saclay.fr (L. Salmon).

https://doi.org/10.1016/j.bioorg.2020.104048
Received 27 January 2020; Received in revised form 26 May 2020; Accepted 24 June 2020
Available online 29 June 2020

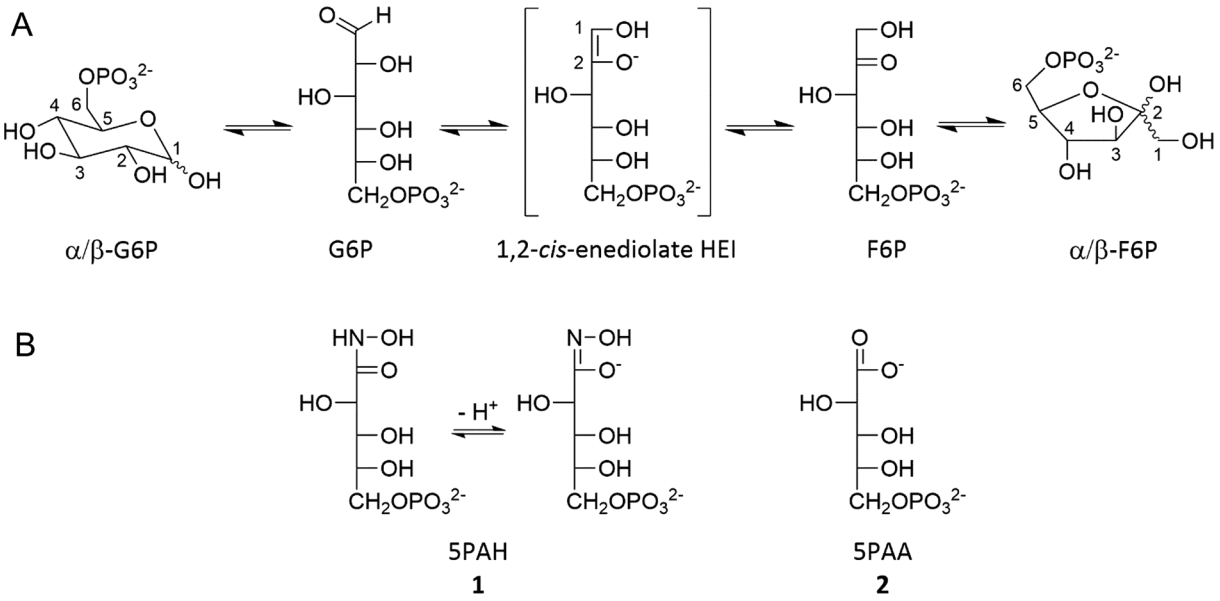

Scheme 1. (A) Reversible reaction catalyzed by phosphoglucose isomerase (PGI) between α/β-D-glucopyranose 6-phosphate (α/β-G6P) and α/β-D-fructofuranose 6-phosphate (α/β-F6P) through the 1,2-*cis*-enediolate high-energy intermediate (HEI). (B) Representation of 5-phosphate-D-arabinonohydroxamic acid (5PAH, **1**) [3] and 5-phospho-D-arabinonate (5PAA, **2**) [4], two strong PGI inhibitors reported as HEI analogues.

discovered independently, in terms of sequence and 3D structure [5,27], human AMF is identical to human PGI but with different functionalities and locations. Through activation of the AMF membrane receptor (AMFR) of tumor cells, AMF has been shown to decrease cell adhesion and to induce their motility [21,28]. For the purpose of designing new, specific, sensitive and non-invasive diagnostic tools for the early detection of an ongoing cancer process, we are looking for suitable bioreceptor molecules that could be grafted onto an electrode for efficient electrochemical detection of AMF in urine and/or serum of cancer patients. Because the AMF recognition site involves, at least in part, the active site of human PGI, enzyme substrates and competitive inhibitors might be used as bioreceptors. Indeed, we designed a highly efficient carbohydrate-based electrochemical biosensor with sensitivity in the pM range using the PGI substrate F6P [29].

In order to find new strong AMF-PGI inhibitors that could be potentially used as anticancer agents and/or as bioreceptors for carbohydrate-based electrochemical biosensors, we report in this study the synthesis and kinetic evaluation of several new human PGI inhibitors derived from the synthon 5-phospho-D-arabinono-1,4-lactone **3** and primary amines **4a-k** to afford the corresponding *N*-substituted 5-phosphate-D-arabinonamide derivatives **5a-k** (Scheme 2). Although not designed as HEI analogue inhibitors of the enzyme catalyzed isomerization reaction, several of these compounds appear as new strong PGI inhibitors, including *N*-(5-phosphate-D-arabinoyl)-2-(amino)ethanamine (5PAED, **5j**, Scheme 2) for which we report a K_i value of 0.7 μM, and the crystal structure at 2.38 Å resolution of its complex with AMF-PGI (we previously reported the use of 5PAED **5j** in a biosensor for AMF detection in a separate detailed electrochemical study [30]). Analysis of the active site interactions, in addition to kinetic evaluations of several of the new inhibitors synthesized in this study, clearly shows that AMF-PGI is able to accept a rather large modification of the C-1 "head" part of the ligand bound at the PGI active site.

All of these compounds **5a-k** (Scheme 2) were also evaluated as potential inhibitors of type I zinc(II) phosphomannose isomerase (PMI), the enzyme that reversibly catalyzes the isomerization of D-mannose 6-phosphate (M6P, epimer of G6P on C-2) to F6P [31]. Indeed, 5PAH (**1**, Scheme 1) is known to strongly inhibit both PGI [3] and PMI [32] catalyzed isomerization reactions. Therefore, the discovery of PGI-specific inhibitors that do not inhibit PMI is of obvious therapeutic interest. Indeed, none of the synthesized compounds **5a-k** seem to be

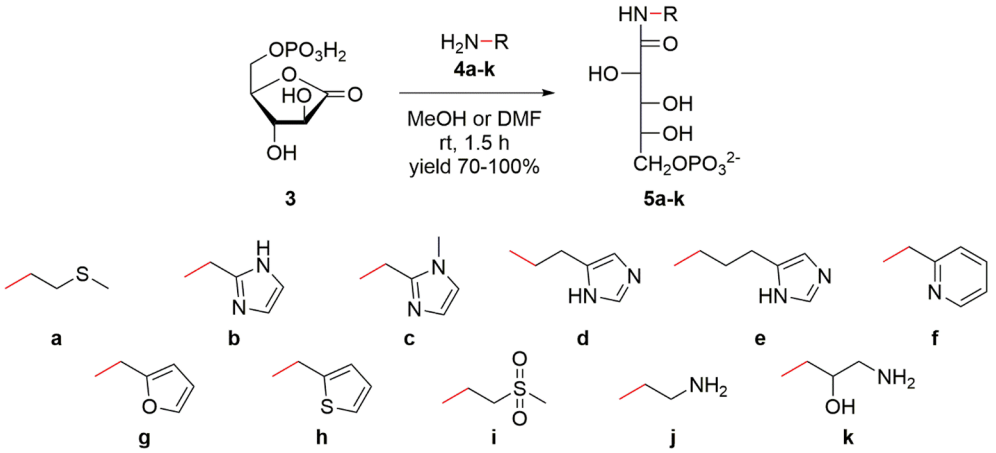

Scheme 2. Synthesis of *N*-substituted 5-phosphate-D-arabinonamide derivatives **5a-k** through nucleophilic addition of the respective primary amines **4a-k** on the synthon 5-phospho-D-arabinono-1,4-lactone **3**.

PMI inhibitors. Contrarily to PGI, the PMI active site does accommodate only substrate or true HEI analogues.

2. Results and discussion

2.1. Chemistry

N-Substituted 5-phosphate-D-arabinonamide derivatives **5a-k** were all obtained by reaction of the respective commercially available primary amines **4a-k** on 5-dihydrogeno-phospho-D-arabinono-1,4-lactone **3** [3,33] through nucleophilic substitution and subsequent ring opening in anhydrous MeOH (except **5f** which was synthesized in anhydrous DMF for solubility reasons) upon stirring 1.5 h at room temperature (Scheme 2). Following concentration of the reaction mixture, ion-exchange chromatography followed by lyophilization afforded pure *N*-substituted 5-phosphate-D-arabinonamide derivatives **5a-k** in yields ranging from 70 to 100%. All compounds were fully characterized by ^{1}H, ^{13}C, and ^{31}P NMR, and high-resolution mass spectrometry analyses (see Experimental section).

2.2. Inhibition kinetics

N-Substituted 5-phosphate-D-arabinonamide derivatives **5a-k** were first evaluated as potential inhibitors of PMIs from *Escherichia coli* (EcPMI, Sigma-Aldrich) and *Candida albicans* (CaPMI) [31] on the M6P to F6P isomerization reaction [34]. IC_{50} values ranging from 1600 to 175 μM were obtained (see Supp. Info. SI1), which shows that none of these compounds behave as good PMI inhibitors in comparison to K_M values for M6P of 330 μM [35] and 200 μM [36], respectively.

As illustrated in Table 1, compounds **5a-k** appear to be inhibitors of both rabbit muscle and human PGI [30] catalyzed isomerization reactions [37], with IC_{50} values ranging from 30 (**5a** vs. RmPGI) to 0.91 μM (**5j** vs. hPGI), in comparison to K_M values for F6P = 60 μM and 50 μM, respectively. As could be expected from their high sequence similarity (93%), the kinetic parameters are similar for both PGIs.

Surprisingly compounds **5c**, **5d**, **5f**, and **5g** are rather good PGI inhibitors with respective IC_{50} values of 3.1, 4.9, 2.9, and 1.5 μM (vs. hPGI), despite the fact that their *N*-substituted *N*-methyl-methylimidazolyl) (**5c**), ethylimidazolyl (**5d**), 2-methylpyridyl (**5f**), and 2-methylfuranyl (**5g**) amide groups on C-1 are rather voluminous. A hypothesis could be that their aromatic substituents interact favorably with the positively charged Arg272 residue at the active site through well-documented favorable cation-π interactions [38,39]. Other compounds with aromatic substituents display slightly higher IC_{50} values for RmPGI of 11 μM (methylimidazolyl, **5b**), 15 μM (propylimidazolyl, **5e**), and 14 μM (methylthiofuranyl, **5h**). These small IC_{50} differences between aromatic compounds are difficult to rationalize. When compared to **5c** (methyl-methylimidazolyl) and **5f** (2-methylpyridyl) which are similar in size, **5e** (propylimidazolyl) bears a longer substituent on C-1 which could impair its cation-π energy interaction versus Arg. Also, compound **5b** (methylimidazolyl) is not as good an inhibitor as **5c** (methyl-methylimidazolyl) probably because of a lower cycle electron density. Compounds bearing non-aromatic substituents display higher IC_{50} values with 30 μM (methylethylsulfide, **5a**), and 13 μM (methylethylsulfone, **5i**), except for **5j** and **5k** which are particular cases. Indeed, these two compounds bearing ethylamino (**5j**, 5PAED) and β-hydroxypropylamino (**5k**, 5PADP) *N*-substituted amide groups were originally designed to interact favorably with negatively charged Glu357 active site residue, their primary amino group being most likely protonated at physiological pH. Compounds **5j** and **5k** appear as new strong PGI inhibitors, with respective IC_{50} values of 1.00 and 2.86 μM vs. RmPGI, and 0.91 and 0.95 μM vs. hPGI. It is noteworthy that these values are quite close to those we measured for 5PAH (**1**) and 5PAA (**2**), respectively 0.80 and 0.46 μM in our experimental conditions (50 mM HEPES, pH 7.1, 25 °C). The remarkable point is that 5PAED (**5j**) and 5PADP (**5k**) are not HEI analogue inhibitors, contrarily to 5PAH (**1**) and 5PAA (**2**). Obviously, unexpected but favorable interactions must take place at the active site with 5PAED (**5j**) and 5PADP (**5k**), as illustrated below by the crystal structure of hPGI-5PAED complex. Favorable electrostatic interactions probably take place between the protonated Arg residue at the active site and the non-protonated amino group of inhibitors **5j** (ethylamino) and **5k** (β-hydroxypropylamino).

The inhibition constants (K_i) were measured for the best three hPGI inhibitors **5g**, **5j**, and **5k** vs. RmPGI and hPGI. Surprisingly, Lineweaver-Burk representation of the initial velocity V_o as a function of F6P concentration at various inhibitor concentrations reveals that these inhibitors are indeed mixed inhibitors (see Supp. Info. SI2), with respective K_i values = 1.5, 0.7, and 0.5 μM, and K_i' values = 5.0, 2.3, and 2.6 μM for hPGI (Table 1). In our experimental conditions, these compounds bind not only to the free enzyme E (K_i), but also to the enzyme-substrate complex ES (K_i'). Substrate binding to PGI probably allows the inhibitor to bind to an allosteric site. However, we suspect that the inhibitor only binds to the active site of the enzyme, as shown by the crystallographic study presented below for the complex hPGI-

Table 1
Kinetic parameters describing the inhibition of rabbit muscle and human phosphoglucose isomerases with compounds **1**, **2** and **5a-k.**[a]

	IC_{50} (μM)		K_i (μM)		K_i' (μM)
Inhibitor	RmPGI	hPGI	RmPGI	hPGI	hPGI
1 [b]	0.888 ± 0.006	0.796 ± 0.006	0.21 ± 0.06[c]	0.19 ± 0.06	–
2 [b]	0.450 ± 0.005	0.456 ± 0.002	0.39 ± 0.08 [d]	0.15 ± 0.08	–
5a	30 ± 2	[e]	[e]	[e]	[e]
5b	11.0 ± 0.3	[e]	[e]	[e]	[e]
5c	3.95 ± 0.05	3.10 ± 0.08	[e]	[e]	[e]
5d	5.2 ± 0.2	4.93 ± 0.08	[e]	[e]	[e]
5e	15.0 ± 0.7	[e]	[e]	[e]	[e]
5f	5.4 ± 0.3	2.9 ± 0.3	[e]	[e]	[e]
5g [f]	2.6 ± 0.3	1.5 ± 0.2	3.2 ± 0.6	1.5 ± 0.2	5.04 ± 0.08
5h	13.9 ± 0.4	[e]	[e]	[e]	[e]
5i	13.2 ± 0.3	[e]	[e]	[e]	[e]
5j [f]	1.00 ± 0.02	0.91 ± 0.09	1.0 ± 0.1	0.7 ± 0.1	2.3 ± 0.1
5k [f]	2.86 ± 0.02	0.95 ± 0.05	[e]	0.52 ± 0.07	2.6 ± 0.4

[a] Conditions: 50 mM HEPES buffer, pH 7.1, 25 °C (RmPGI: rabbit muscle phosphoglucose isomerase, hPGI: human phosphoglucose isomerase);
[b] Competitive inhibition;
[c] In ref. [3]: K_i = 0.195 ± 0.006 μM (50 mM TRIS HCl buffer, pH 8.0, 30 °C);
[d] In ref. [4]: K_i = 0.46 μM (100 mM MOPS buffer, pH 7.0, 30 °C);
[e] Value not determined;
[f] Mixed inhibition.

5PAED (**5j**). Such sub-micromolar K_i values measured for **5j** and **5k** are only slightly higher than the K_i values we measured for the competitive inhibitors 5PAH (**1**) and 5PAA (**2**), respectively 0.19 and 0.15 μM. Although not designed as HEI analogue inhibitors, **5j** (5PAED) and **5k** (5PADP) appear to be new strong PGI inhibitors with K_M/K_i ratios (hPGI) equals about 70 and 100, respectively. Interestingly, the crystallographic study described below will show an expected binding mode of 5PAED (**5j**) at the hPGI active site.

2.3. Crystallographic studies

Co-crystallization of hPGI in complex with 5PAED (**5j**) gave rod shaped crystals that belonged to the space group symmetry $P4_3$ ($a = b = 96.110$ Å, c = 271.450 Å) (Supp. Info. SI3). X-ray diffraction data were collected at PROXIMA 2 beamline (SOLEIL) and the structure was solved at 2.38 Å (PDB code 6XUH) by molecular replacement using the coordinates of the hPGI crystal structure (PDB 1IAT) [5]. The asymmetric unit contains four copies of PGI. Two form a biological dimer and the other two form dimers through crystallographic symmetry axes (the protein is only active in dimeric form [40]). PGI contains 556 amino acids and is composed of a large and a small domain. The large *N*-terminal domain is formed by four parallel and two antiparallel β strands surrounded by α helices. The small domain contained between the residues 115–288 is made by a five parallel β-stranded sheet surrounded by α helices. A third domain formed by residues 511–556 extends towards the other monomer. The active site is located between the C-terminal domain and the small domain. Each of the two active sites of the homodimer is composed of amino acids of one monomer and the His388 residue of the other monomer (Fig. 1A).

The binding mode of the 5PAED compound (**5j**) to hPGI was not completely as expected. While a 5PAED (**5j**) molecule was unambiguously bound in the active site of one subunit of the homodimer (Fig. 1B), the residual electron density at the other subunit did not correspond to 5PAED. We interpreted this density as a bound 5PAA (**2**) moiety (Fig. 1A). Similarly, one molecule of 5PAED (**5j**) and one molecule of 5PAA (**2**) are found in each of the other two monomers in the asymmetric unit. The co-crystallization process extended over a period of 17 days which likely allowed 5PAED (**5j**) to decompose to 5PAA (**2**) and ethylenediamine, either by hydrolysis or by reversible formation of the lactone precursor **3**, which further hydrolyzed to 5PAA (**2**). Indeed, we checked by NMR analysis (see Supp. Info SI4) that 5PAED (**5j**) was stable enough in aqueous medium for kinetic evaluation of its inhibitory properties, but most likely not sufficiently stable to avoid partial decomposition during the co-crystallization process. Upon soaking of hPGI crystals in mother liquid containing 5PAED, we exclusively identified 5PAA bound at the enzyme active sites. 5PAED (**5j**) most likely entirely decomposed to 5PAA (**2**) during the one-day equilibration time of a 5 mM 5PAED drop against the crystallization buffer or during the subsequent 8 h soaking time of the hPGI crystals in the equilibrated inhibitor drop. The structure of hPGI-5PAA (**2**) was solved at 1.95 Å (PDB code 6XUI). Except for the locations of water molecules, the 3D structure is identical to the deposited hPGI-5PAA 2.5 Å structure (PDB code 1NUH) [10], and also very similar to the 1.9 Å rabbit muscle PGI-5PAA (RmPGI-5PAA) structure (PDB code 1G98) [9], and will therefore not be further described. Fig. 2 shows an overview of the interactions of 5PAED (**5j**) with active site residues of hPGI. The residues correspond to those identified in other PGI structures such as RmPGI-5PAA (PDB code 1G98), RmPGI-5PAH (PDB code 1KOJ) and hPGI-5PAA (PDB code 1NUH) [8–10]. The same residues are found at the active site with, in addition, the implication of Gly271. Eleven residues form the active site of the enzyme and provide a network of hydrogen bonds with 5PAED (**5j**), including six residues (Ser159, Ser209, Lys210, Lys518, Thr211 and Thr214) which anchor the phosphoryl group, showing its importance for binding of the inhibitor. Ser159 is involved in a H-bond with an oxygen atom (2.9 Å) of the phosphoryl group via its hydroxyl group. This same oxygen is interacting with the Cα nitrogen of Lys210 at a distance of 2.9 Å. Another oxygen atom of the phosphoryl group establishes three H-bonds at distances of 2.9, 2.0 and 3.1 Å respectively with the hydroxyl groups of Ser209 and the two threonine's Thr214 and Thr211. The latter also interacts via its NH group with another oxygen atom of the phosphoryl group at a distance of 3.1 Å. Lys518 is in interaction with O5 oxygen atom of the phosphoryl group. Indeed, and according to the structure of RmPGI with F6P (PDB 1HOX) [7], this lysine, which does not interact directly with the substrate in its cyclic form, approaches after opening of the cycle to interact with the substrate under its linear form. This structure supports the results already described in the literature highlighting the importance of phosphoryl group in the anchoring of the inhibitor.

The hPGI-5PAED structure confirms that Glu357 is correctly positioned to act as the catalytic base of the isomerization process. Glu357 is in interaction with nitrogen N1 (2.6 and 2.9 Å) of 5PAED which corresponds to the C1 carbon of the substrate F6P and is at a distance of 3.3 Å of the atom corresponding to the C2 of G6P: it is at the level of

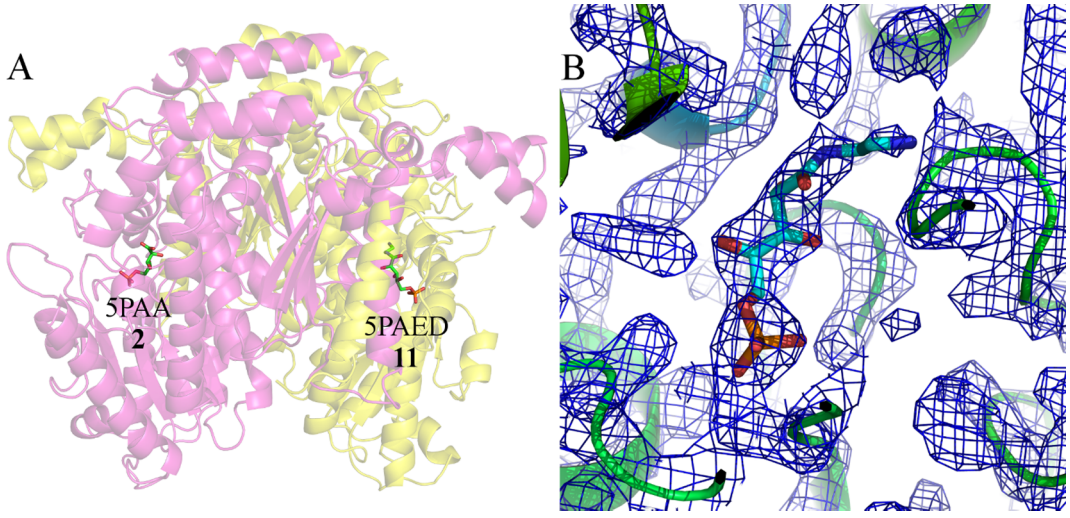

Fig. 1. (A) Three-dimensional X-ray crystal structure of the complex between homodimeric human phosphoglucose isomerase (cartoon presentation with one subunit colored in pink and the other in yellow) and inhibitors 5-phospho-D-arabinonate (5PAA, **2**) and *N*-(5-phosphate-D-arabinoyl)-2-(amino)ethanamine (5PAED, **5j**) respectively located in each of the two enzyme active sites (shown as sticks); (B) omit electron density map at 3σ level, the refined model for 5PAED (**5j**) is shown as sticks. (For interpretation of the references to colour in this figure legend, the reader is referred to the web version of this article.)

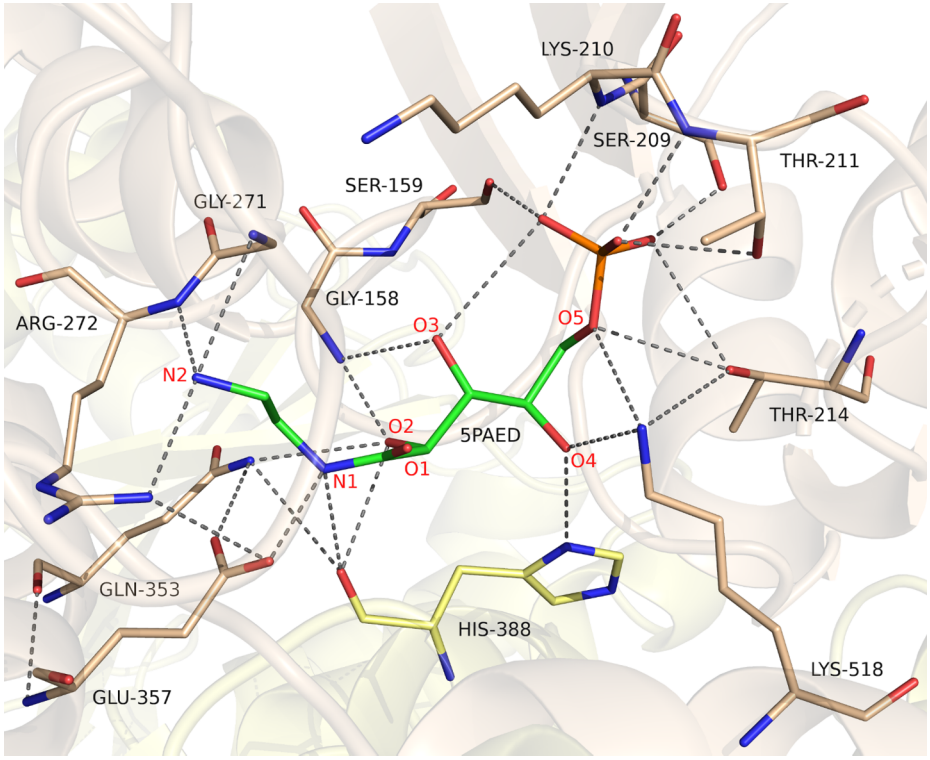

Fig. 2. Representation of the active site of human phosphoglucose isomerase (hPGI) in complex with *N*-(5-phosphate-D-arabinoyl)-2-(amino)ethanamine (5PAED, **5j**). Only amino acids directly in interaction with the inhibitor are depicted. H-Bonds are drawn as grey dashed lines (H-bond distances were omitted for clarity, but are available in Supp. Info. SI5). Residues of monomer A are shown in light brown, and that of monomer B (His388) are shown in pale yellow. (For interpretation of the references to colour in this figure legend, the reader is referred to the web version of this article.)

these two carbon atoms that the catalytic base pulls the hydrogen from the substrate to bring to the 1,2-*cis*-enediolate HEI. Gly271, for its part, establishes a hydrogen bond with N2 nitrogen of 5PAED [d(NH-N2) = 2.9 Å]. Arg272 is also well positioned to interact with this same nitrogen. The latter is probably unprotonated (NH_2 form, pK_a ~ 9) so that it can interact with the nitrogen of arginine, which is very probably protonated at the active site (pK_a ~ 12). This structural study shows that, contrary to what we initially postulated, the terminal amine functional group of 5PAED does not interact with Glu357 via an ionic bond, but establishes three H-bonds with Arg272 and Gly271 (from one monomer). The polyhydroxylated skeleton participates via four H-bonds when mooring the inhibitor at the active site. His388 (from the second monomer) participates in two of these H-bonds: it interacts via its carbonyl and the imidazole nitrogen with the two oxygen atoms O2 (2.6 Å) and O4 (3.0 Å), respectively, of 5PAED (**5j**). The latter corresponds to the O5 cyclic oxygen atom of F6P, which confirms the role attributed to His388 derived from the structure of RmPGI-F6P (PDB 1HOX) [7]: His388 catalyzes the ring opening step of the cyclic substrate by protonating the F6P furanose oxygen or pyranose G6P atom. Gly158 completes the hydrogen bonding network by interacting via its nitrogen with the O2 and O3 oxygen atom of the inhibitor.

Detailed structural alignments of the hPGI-5PAED (**5j**) structure with those of RmPGI-5PAH (**1**) (PDB code 1KOJ, [8]) depicted in Fig. 3A and RmPGI-5PAA (**2**) (PDB code 1G98, [9]) depicted in Fig. 3B show small but significant differences. Indeed, Lys518 that interacts with O4 and O5 oxygen atoms of inhibitors 5PAH (Fig. 3A) or 5PAA (Fig. 3B), reorients to interact with O4 and the Thr214 side chain oxygen atom. Another important observation can be made: the good superposition of the terminal $-NH_2$ functional group of the 5PAED of the hPGI-5PAED structure with the hydroxyl group of the −NHOH functional group (distance 1.5 Å) of the hPGI-5PAH complex structure (Fig. 3A). This hydroxamic acid functional group provides two H-bonds with the two nitrogen atoms of Arg272. It is replaced by the NH_2 group of 5PAED (**5j**) which, in addition to interacting with Arg272 via two H-bonds, involves an additional third H-bond to Gly271. In the case of the RmPGI-5PAA structure (Fig. 3B), a water molecule is well-positioned between the carboxylate functional group of 5PAA and Arg272, also offering two H-bonds to this residue. Here again one can observe a good superposition of the terminal $-NH_2$ functional group of 5PAED with this water molecule (distance 1.0 Å).

Overall, the crystallographic study of the hPGI-5PAED complex shows that the active site of PGIs, and more particularly of hPGI is relatively tolerant for modification of the head "C-1" part of its inhibitors, unlike PMIs. This observation is supported by kinetic assays which gives K_i values in the same order of magnitude for 5PAH (**1**), 5PAA (**2**), and 5PAED (**5j**), respectively 0.19, 0.15, and 0.7 μM.

3. Conclusions

In conclusion, we report the synthesis of new potentially anti-metastatic compounds, that are good to excellent inhibitors of hPGI-AMF and which do not mimic the 1,2-*cis*-enediolate functional group of the HEI involved in the F6P to G6P isomerization reaction, both in terms of coplanarity and steric hindrance. One of these new PGI inhibitors, namely *N*-(5-phosphate-D-arabinoyl)-2-(amino)ethanamine (5PAED, **5j**) displays a low K_i value = 0.7 μM. The X-ray structure of this inhibitor within the hPGI-AMF active site was resolved at 2.38 Å resolution and showed its unexpected mode of interaction at the active site of the enzyme and explained its strong inhibitory power. Overall, the crystallographic study of the hPGI-5PAED complex shows that the active site of PGIs, and more particularly of hPGI, as supported by kinetic assays, is relatively tolerant for modification of the head "C-1" part of its inhibitors, unlike other aldose-ketose isomerases like PMIs. The fact that hPGI inhibitors might be functionalized at the head C-1 part offers the possibility of future design of original bioreceptors to be grafted on biosensors for the efficient detection of the cancer biomarker AMF-PGI. We recently reported such a biosensor using 5PAED (**5j**) as bioreceptor [30]. Here, we demonstrate how such a bioreceptor could interact at the active site of hPGI and open the door to the development of future original carbohydrate-based biosensors for the early detection of biomarkers of therapeutic interest.

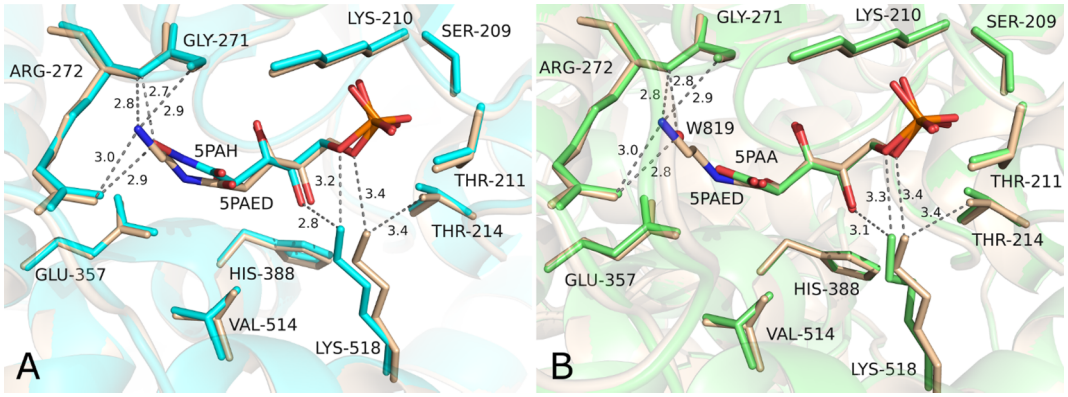

Fig. 3. Active site view of the structural alignments of human phosphoglucose isomerase (hPGI) in complex with *N*-(5-phosphate-D-arabinoyl)-2-(amino)ethanamine (5PAED, **5j**) depicted in light brown and: (A) rabbit muscle PGI in complex with 5-phosphate-D-arabinonohydroxamic acid (5PAH, **1**, light blue, PDB 1KOJ [8]); (B) rabbit muscle PGI in complex with 5-phospho-D-arabinonate (5PAA, **2**, light green, PDB 1G98 [9]). Some amino acids were omitted for clarity. H-Bonds are drawn as dashed lines and distances are given in angstrom. (For interpretation of the references to colour in this figure legend, the reader is referred to the web version of this article.)

4. Experimental section

4.1. Chemistry

4.1.1. Reagents and methods

All chemical reagents were of analytical grade, obtained from Sigma Aldrich, and used without further purification. Solvents were obtained from SDS or VWR. MeOH was dried by refluxing with Mg/I_2, then distilled and used immediately. Flash chromatography was performed using silica gel (35–70 μm, E. Merck) under N_2 pressure. Unless otherwise stated, all organic extracts were dried over Na_2SO_4 and filtered. Concentration of solutions was performed under diminished pressure at temperature < 30 °C using rotary evaporator. All air- and moisture-sensitive reactions were performed under an atmosphere of argon. Analytical TLC was performed using Silica Gel 60 F_{254} precoated aluminum plates (E. Merck). Spots were visualized by treatment with 5% ethanolic H_2SO_4 followed by heating and/or by absorbance of UV light at 254 nm. NMR spectra (see Supp. Info. SI6) were recorded at 297 K in D_2O with Bruker DRX 300 (^{1}H at 300.13 MHz and ^{13}C at 75.47 MHz) or DPX 250 (^{1}H at 250.13 MHz, ^{13}C at 62.90 MHz, and ^{31}P at 101.26 MHz) spectrometer using NMR Notebook 2.0 WinNMR software. Chemical shifts are reported in ppm (δ) and coupling constants in Hz (J_{ij}). ^{1}H NMR spectra were referenced to internal residual HOD (δ 4.78). ^{13}C NMR spectra were referenced to dioxane (δ 67.4). In most cases, COSY, HSQC, and/or DEPT135 NMR spectra were recorded for assigning resonances. Infrared spectra were recorded with a FTIR Bruker IFS-66 spectrometer. High-resolution mass spectrometry (HRMS) analyses were performed by electrospray with negative (ESI^-) ionization mode.

4.1.2. General procedure for the synthesis of N-substituted 5-phosphate-D-arabinonamide derivatives **5a-k**

In a round-bottom flask placed under argon, containing D-arabinono-1,4-lactone 5-phosphate **3** (0.50 mmol) in 5 mL anhydrous methanol (DMF for **5f** synthesis), primary amine **4a-k** (2.0 mmol, 4 eq) was added. The reaction mixture was stirred at rt for 1.5 h. Following concentration of the reaction mixture, the residue was eluted with water on a Dowex 50WX4 ion-exchange column (100–200 mesh, Na^+ form) and lyophilized to afford the target compound **5a-k**.

*4.1.2.1. N-(5-Phosphate-D-arabinoyl)-2-(methylsulfanyl)ethanamine (5PAMC, **5a**).* White solid, 100% yield; FTIR ν (cm^{-1}) 3500–3200 (OH, NH), 2990–2800 (CH, CH_2), 1643 (C═O), 1541 (NH), 1086 (P—O, C—O), 976 (P—O); ^{1}H NMR (D_2O, 300 MHz) δ_H 4.38 (s, 1H, H_2), 3.93–3.76 (m, 4H, H_3 + H_4 + H_5 + $H_{5'}$), 3.41 (m, 2H, H_6), 2.62 (m, 2H, H_7), 2.06 (s, 3H, H_8); ^{13}C NMR (D_2O, 75 MHz) δ_C 175.5 (C-1), 70.9 (C-3), 70.7 (C-2), 69.8 (C-4), 65.1 (C-5), 37.9 (C-6), 32.4 (C7), 14.2 (C-8); ^{31}P NMR (D_2O, 121.5 MHz) δ_P 4.7 ppm; HRMS (ESI-) *m/z*: Calcd for $C_8H_{17}NO_8PS$ $[M-2Na+H]^-$ 318.0413, Found 318.0420.

*4.1.2.2. N-[(5-Phosphate-D-arabinoyl)-1-(imidazol-2-yl)methanamine (5PAIm, **5b**).* White solid, 100% yield; FTIR ν 3500–3200 (OH, NH), 3000–2820 (CH, CH_2, CH_{arom}), 1652 (C═O), 1544 (NH), 1436 (C═C), 1089 (P—O, C—O, C—N), 975 (P—O) cm^{-1}; ^{1}H NMR (D_2O, 300 MHz) δ_H 6.96 (m, 2H, H_8 + H_9), 4.45 (m, 3H, H_2 + H_6 + $H_{6'}$), 3.99–3.78 (m, 4H, H_3 + H_4 + H_5 + $H_{5'}$) ppm; ^{13}C NMR (D_2O, 75 MHz) δ_C 176.0 (C-1), 144.8 (C-7), 122.0 (C-8, C-9), 71.0 (C-3), 70.9 (C-2), 69.9 (d, $JC_{4,P}$ = 4.6 Hz), 65.0 (C-5), 36.3 (C6) ppm; ^{31}P NMR (D_2O, 121.5 MHz) δ_P 4.9 ppm; HRMS (ESI-) *m/z*: Calcd for $C_9H_{15}N_3O_8P$ $[M-2Na+H]^-$ 324.0597, Found 324.0600.

*4.1.2.3. N-(5-Phosphate-D-arabinoyl)-1-(1-methylimidazol-2-yl) methanamine (5PAMIm, **5c**).* Brown solid, 100% yield; FTIR ν (cm^{-1}) 3500–3200 (OH, NH), 3000–2800 (CH, CH_2, CH_{arom}), 1648 (C═O), 1534 (NH), 1451–1417 (C═C), 1091 (P—O, C—O, C—N), 977 (P—O); ^{1}H NMR (D_2O, 300 MHz) δ_H 6.97 (s, 1H, H_8), 6.83 (s, 1H, H_9), 4.43–4.40 (m, 3H, H_2 + H_6 + $H_{6'}$), 3.88–3.72 (m, 4H, H_3 + H_4 + H_5 + $H_{5'}$), 3.50 (s, 2H, H_{10}); ^{13}C NMR (D_2O, 75 MHz) δ_C 176.6 (C-1), 144.5 (C-7), 126.0 (C-8), 122.8 (C-9), 71.5 (C-3), 71.2 (C-2), 70.3 (d, C-4, $JC_{4,P}$ = 5.2 Hz), 65.2 (C-5), 35.0 (C-6), 32.5 (C-10); ^{31}P NMR (D_2O, 121.5 MHz) δ_P 4.8 ppm; HRMS (ESI-) *m/z*: Calcd for $C_{10}H_{17}N_3O_8P$ $[M-2Na+1H]^-$ = 338.0754, Found 338.0756.

*4.1.2.4. N-(5-Phosphate-D-arabinoyl)histamine (5PAHis, **5d**).* Light brown solid, 80% yield; FTIR ν (cm^{-1}) 3500–3200 (OH, NH), 3000–2850 (CH, CH_2, CH_{arom}), 1642 (C═O), 1547 (NH), 1434 (C═C), 1085 (P—O, C—O, C—N), 974 (P—O); ^{1}H NMR (D_2O, 300 MHz) δ_H 7.64 (s, 1H, *H*10), 6.86 (s, 1H, H_9), 4.34 (s, 1H, H_2), 3.92–3.90 (m, 4H, H_3 + H_4 + H_5 + $H_{5'}$), 3.40 (s, 2H, H_6), 2.72 (s, 2H, H_7); ^{13}C NMR (D_2O, 75 MHz) δ_C 175.3 (C-1), 135.7 (C-10), 134.3 (C-8), 117.0 (C-9), 70.9 (C-3), 70.7 (C-2), 69.9 (d, C-4, $JC_{4,P}$ = 5.2 Hz), 65.0 (C-5), 38.8 (C-6), 25.8 (C-7); ^{31}P NMR (D_2O, 121.5 MHz) δ_P 4.8 ppm; HRMS (ESI-) *m/z*: Calcd for $C_{10}H_{16}N_3NaO_8P$ $[M-1Na]^-$ 362.0730, Found 362.0715.

*4.1.2.5. N-(5-Phosphate-D-arabinoyl)-3-(imidazol-1-yl)propanamine (5PAPIm, **5e**).* Light brown solid, 70% yield; FTIR ν (cm^{-1}) 3500–3200 (OH, NH), 3000–2886 (CH, CH_2, CH_{arom}), 1642 (C═O), 1544 (NH), 1446 (C═C), 1083 (P—O, C—O, C—N), 976 (P—O); ^{1}H NMR (D_2O, 300 MHz) δ_H 7.63 (s, 1H, H_{11}), 7.08 (s, 1H, H_{10}), 6.95 (s, 1H, H_9), 4.36

(s, 1H, H_2), 3.96–3.92 (m, 6H, H_3 + H_4 + H_5 + $H_{5'}$+H_8 + $H_{8'}$), 3.14 (s, 2H, H_6), 1.93 (m, 2H, H_7); ^{13}C NMR (D_2O, 75 MHz) δ_C 175.5 (C-1), 137.8 (C-11), 127.3 (C10), 120.1 (C-9), 70.9 (C-3), 70.7 (C-2), 69.9 (d, C-4, $JC_{4,P}$ = 4.9 Hz), 65 (C-5), 44.2 (C-8), 35.9 (C6), 29.6 (C-7); ^{31}P NMR (D_2O, 121.5 MHz) δ_P 4.7 ppm; HRMS (ESI-) *m/z*: Calcd for $C_{11}H_{19}N_3O_8P$ $[M-2Na+H]^-$ 352.0910, Found 352.0914.

*4.1.2.6. N-(5-Phosphate-D-arabinoyl)-1-(pyridin-2-yl)methanamine (5PAPy, **5f**)*. Light brown solid, 100% yield; FTIR ν (cm^{-1}) 3257 (OH, NH), 3000, 2820 (CH, CH_2, CH_{arom}), 1653 (C═O), 1540 (NH), 1400–1595 (C═C), 1097 (P—O, C—O, C—N), 978 (P—O); ^{1}H NMR (D_2O, 250 MHz) δ_H 8.20 (d, 1H, *J* = 6.75 Hz, H_{11}), 7.58 (t, 1H, *J* = 7.25 Hz, H_9), 7.20–7.08 (m, 2H, H_8 + H_{10}), 4.38–4.28 (m, 3H, H_2 + H_6 + $H_{6'}$), 3.88–3.61 (m, 4H, H_3 + H_4 + H_5 + $H_{5'}$); ^{13}C NMR (D_2O, 62.5 MHz) δ_C 177 (C-1), 156.3 (C-7), 148.2 (C-11), 138.2 (C9), 122.8 (C-10), 121.3 (C-8), 71.3 (C-3 et C-2), 70.2 (d, C-4, $JC_{4,P}$ = 4.6 Hz), 65.2 (C-5), 43.8 (C6); ^{31}P NMR (D_2O, 100.3 MHz) δ_P 4.8 ppm; HRMS (ESI-) *m/z*: Calcd for $C_{11}H_{16}N_2O_8P$ $[M-2Na+H]^-$ 335.0645, Found 335.0629.

*4.1.2.7. N-(5-Phosphate-D-arabinoyl)-1-(furan-2-yl)methanamine (5PAF, **5g**)*. Light brown solid, 100% yield; FTIR ν 3500–3200 (OH, NH), 3000–2886 (CH, CH_2, CH_{arom}), 1652 (C═O), 1537 (NH), 1400 (C═C), 1096 (P—O, C—O), 976 (P—O) cm^{-1}; ^{1}H NMR (D_2O, 300 MHz) δ_H 7.43 (s, 1H, H_{10}), 6.37 (s, 1H, H_9), 6.28 (d, 1H, *J* = 3.6 Hz, H_8), 4.44 (s, 2H, H_6 + $H_{6'}$), 4.40 (s, 1H, H_2), 3.98–3.80 (m, 4H, H_3 + H_4 + H_5 + $H_{5'}$) ppm; ^{13}C NMR (D_2O, 75 MHz) δ_C 175.6 (C-1), 151 (C-7), 142.6 (C10), 110.5, 107.2 (C-9, C-8), 70.9 (C-3), 70.8 (C-2), 69.8 (d, C-4, $JC_{4,P}$ = 6.34 Hz), 65.1 (d, C-5, $JC_{5,P}$ = 4.1 Hz), 35.9 (C6) ppm; ^{31}P NMR (D_2O, 121.5 MHz) δ_P 4.5 ppm; HRMS (ESI-) *m/z*: Calcd for $C_{10}H_{15}NO_9P$ $[M-2Na+H]^-$ = 324.0485, Found 324.0491.

*4.1.2.8. N-(5-Phosphate-D-arabinoyl)-1-(thien-2-yl)methanamine (5PAT, **5h**)*. White solid, 100% yield; FTIR ν 3500–3200 (OH, NH), 3000–2879 (CH, CH_2, CH_{arom}), 1646 (C═O), 1530 (NH), 1428 (C═C), 1094 (P—O, C—O), 978 (P—O) cm^{-1}; ^{1}H NMR (D_2O, 300 MHz) δ_H 7.28 (d, 1H, *J* = 4.2 Hz, H_{10}), 6.98–6.95 (m, 2H, H_8 + H_9), 4.55 (s, 2H, H_6), 4.43 (s, 1H, H_2), 4.00–3.81 (m, 4H, H_3 + H_4 + H_5 + $H_{5'}$) ppm; ^{13}C NMR (D_2O, 75 MHz) δ_C 175.4 (C-1), 140.8 (C-7), 127.0 (C10), 125.8, 125.4 (C-9, C-8), 71.0 (C-3), 70.8 (C-2), 69.9 (d, C-4, $JC_{4,P}$ = 4.9 Hz), 65.0 (C-5), 37.6 (C6) ppm; ^{31}P NMR (D_2O, 121.5 MHz) δ_P 4.7 ppm; HRMS (ESI-) *m/z*: Calcd for $C_{10}H_{15}NO_8PS$ $[M-2Na+H]^-$ 340.0256, Found 340.0264.

*4.1.2.9. N-(5-Phosphate-D-arabinoyl)-2-(methylsulfonyl)ethanamine (5PAS, **5i**)*. An anhydrous methanolic solution (2 mL) of NaOMe (129 mg, 2.38 mmol) was prepared under argon. This solution was added through an argon-purged syringe to a methanolic solution (5 mL) of 2-(methylsulfonyl)ethanamine hydrochloride (380 mg, 5 eq) dissolved at 35 ^{0}C. A white solid precipitated (NaCl). Following decantation, the clear methanolic solution of 2-(methylsulfonyl) ethanamine was then transferred dropwise to a MeOH solution (3 mL) of D-arabinono-1,4-lactone 5-phosphate (108 mg, 0.47 mmol) using a second argon-purged syringe. The reaction was allowed to proceed for 1.5 h at rt. General work-up afforded the desired product as a light brown solid (yield = 89%). FTIR ν 3500–3200 (OH, NH), 3000–2879 (CH, CH_2), 1650 (C═O), 1543 (NH), 1090 (P—O, C—O), 974 (P—O) cm^{-1}; ^{1}H NMR (D_2O, 300 MHz) δ_H 4.65 (s, 1H, H_2), 4.08–3.89 (m, 6H, H_3 + H_4 + H_5 + $H_{5'}$+H_7 + $H_{7'}$), 3.63 (m, 2H, H_6), 3.27 (s, 3H, H_8) ppm; ^{13}C NMR (D_2O, 75 MHz) δ_C 175.9 (C-1), 71.2 (C-3), 71 (C-2), 70.0 (C-4), 65.0 (C-5), 53.0 (C-7), 41.0 (C8), 33.0 (C-6) ppm; ^{31}P NMR (D_2O, 121.5 MHz) δ_P 4.7 ppm; HRMS (ESI-) *m/z*: Calcd for $C_8H_{17}NO_{10}PS$ $[M-2Na+H]^-$ 350.0311, Found 350.0320.

*4.1.2.10. N-(5-Phosphate-D-arabinoyl)-2-(amino)ethanamine (5PAED, **5j**)*. White solid, 100% yield; FTIR ν 3500–3200 (OH, NH), 2900, 2820 (CH, CH_2), 1638 (C═O), 1547 (NH), 1090 (P—O, C—O), 976 (P—O) cm^{-1}; ^{1}H NMR (D_2O, 300 MHz) δ_H 4.28 (s, 1H, H_2), 3.85–3.70 (m, 4H, H_3 + H_4 + H_5 + $H_{5'}$), 3.18 (m, 2H, H_6), 2.58 (t, 2H, *J* = 5.4 Hz, H_7) ppm; ^{13}C NMR (D_2O, 75 MHz) δ_C 177.9 (C-1), 71.9 (C-3), 71.5 (C-2), 70.6 (d, C-4, $JC_{4,P}$ = 5.5 Hz), 65.4 (C-5), 41.4 (C-7), 39.8 (C-6) ppm; ^{31}P NMR (D_2O, 121.5 MHz) δ_P 4.6 ppm; HRMS (ESI-) *m/z*: Calcd for $C_7H_{16}N_2O_8P$ 287.0645 $[M-2Na+H]^-$, Found 287.0650.

*4.1.2.11. N-(5-Phosphate-D-arabinoyl)-3-(aminomethyl)ethanolamine (5PADP, **5k**)*. White solid, 81% yield; FTIR ν 3500–3200 (OH, NH), 2900–2820 (CH, CH_2), 1640 (C═O), 1540 (NH), 1089 (P—O, C—O), 977 (P—O) cm^{-1}; ^{1}H NMR (D_2O, 300 MHz) δ_H 4.40 (s, 1H, H_2), 3.75–3.93 (m, 1H, H_3 + H_4 + H_5 + $H_{5'}$+H_7), 3.34 (m, 2H, H_6), 2.60 (m, 2H, H_8) ppm; ^{13}C NMR (D_2O, 75 MHz) δ_C 176.7 (C-1), 71.6 (C-7), 71.2 (C-3, C-2), 70.3 (d, C-4, $JC_{4,P}$ = 5.3 Hz), 65.2 (d, C-5, JC_{5-P} = 4.1 Hz), 43.8 (C-6), 42.4 (C-8) ppm; ^{31}P NMR (D_2O, 121.5 MHz) δ_P 4.8 ppm; HRMS (ESI-) *m/z*: Calcd for $C_8H_{18}N_2O_9P$ $[M-2Na+1H]^-$ 317.0750, Found 317.0754.

4.2. Expression and purification

Human phosphoglucose isomerase (hPGI) was produced according to the procedure we described previously [30].

4.3. Enzymatic assays

Human phosphoglucose isomerase (hPGI) activity was spectrophotometrically assayed according to the procedure reported previously [30].

4.4. Crystallisation and data collection

Crystals of human PGI (alone or in complex with 5PAED (**5j**)) were produced by mixing concentrated protein (8 mg mL^{-1}) without or with 5 mM of 5PAED (in 50 mM sodium chloride, 20 mM Tris, pH 7.5) with crystallization buffer (28–32% PEG 4000, 200 mM magnesium chloride, 100 mM Tris, pH 8.5) in a 1:1 ratio. Drops (2 µL) were equilibrated against a well of 500 µL crystallization solution at 18 °C by the hanging-drop vapor-diffusion method. Crystals from hPGI obtained in presence of 5PAED were cryoprotected in 33% PEG4000, 0.2 M magnesium chloride, 0.1 M Tris, pH 8.5, 15% glycerol and 5 mM 5PAED before flash cooled in liquid nitrogen. Diffraction data were collected at the Proxima 2 beam line, synchrotron SOLEIL (Gif-sur-Yvette, France), at 100 K on a EIGER X 9 M area detector. The crystal belongs to space group $P4_3$ with cell dimensions $\boldsymbol{a}$ = $\boldsymbol{b}$ = 96.110 Å and $\boldsymbol{c}$ = 271.450 Å and contains four PGI molecules per asymmetric unit (see Supp. Info. SI3), with an estimated solvent content of 42.4%. Crystals from hPGI alone were also soaked 8 h in a buffer containing 5 mM of 5PAED (in 50 mM sodium chloride, 20 mM Tris, pH 7.5). They were cryoprotected in 32.5% PEG4000, 0.1 M magnesium chloride, 0.1 M Tris, pH 8.5, 13.9% glycerol and 5 mM 5PAED and flash cooled in liquid nitrogen. Diffraction data were collected at the Proxima 1 beam line, synchrotron SOLEIL (Gif-sur-Yvette, France), at 100 K on a Dectris Pilatus 6 M detector. The hPGI crystal soaked with 5PAED belongs to space group $P2_12_12_1$ with cell dimensions $\boldsymbol{a}$ = 80.55 Å, $\boldsymbol{b}$ = 106.95 Å, $\boldsymbol{c}$ = 270.40 Å and contains four PGI molecules per asymmetric unit, with an estimated solvent content of 47.8%. Data were indexed and processed with XDS [41] (Table 2).

4.5. Structure determination and refinement statistics

Structure of hPGI-5PAED complex was solved by molecular replacement (program PHASER) [42] using the structure of hPGI at 1.6 Å resolution (PDB code 1IAT). The model was build semi-automatically after density modification using Parrot, REFMAC5 and BUCCANEER [43]. At this step (for the hPGI-5PAED complex), 2112 residues were

Table 2
Crystallographic data collection and refinement statistics of hPGI-5PAED (**5j**) complex.

Crystallographic data collection		
	hPGI-5PAED (**1**)	hPGI-5PAA (**2**)
X-ray source	PROXIMA 2	PROXIMA 1
Wavelength (Å)	0.9801	0.97857
Temperature (K)	100	100
Unit-cell parameters (Å, °)	$\boldsymbol{a}$ = 96.11, $\boldsymbol{b}$ = 96.11, $\boldsymbol{c}$ = 271.45, $\boldsymbol{\alpha}$ = $\boldsymbol{\beta}$ = γ = 90.0	$\boldsymbol{a}$ = 80.55, $\boldsymbol{b}$ = 106.95, $\boldsymbol{c}$ = 270.4, $\boldsymbol{\alpha}$ = $\boldsymbol{\beta}$ = γ = 90.0
Space group	$P4_3$	$P2_12_12_1$
Resolution limits† (Å)	47.32–2.38 (2.52–2.38)	48.26–1.95 (2.07–1.95)
Number of observations†	339425(53656)	627727(98542)
Number of unique reflections	97562(15379)	170097(26904)
R-meas† (%)	11.9(97.4)	10.9(111.7)
Completeness† (%)	99.2(97.0)	99.3(98.1)
I/σ† (I)	8.12(1.57)	10.40(1.33)
CC (1/2)	99.5(82.1)	99.8(65.3)
Refinement statistics		
Number of non-hydrogen atoms (protein/ligands/water)	17748/66/271	17748/144/1469
R/R_{free} (%)	26.61/31.69	17.07/21.93
R.M.S.D. Bonds (Å)/angles (°)	0.01/1.44	0.02/1.85
Average temperature factors (protein/ligands/waters)	75.26/64.6/42.5	31.29/44.13/38.56

† Values in parentheses refer to the highest resolution shell: 2.52–2.38 or 2.07–1.95 for the co-crystal or the soaked complex, respectively.

uniquely allocated to 4 chains (90.3% of completeness by residues built) with a FOM value of 0.86 and R/Rfree = 30/35. The model was further improved by iterative cycles of manual rebuilding using COOT [44] and refinement using REFMAC5 program [45]. This yielded a R/R_{free} factor of 26/32%. The final model contains 4 chains of residues 1–556, 2 molecules of 5PAED, 2 molecules of 5PAA and 271 water molecules. The structure of the hPGI soaked with 5PAED was solved using the same protocol and we observed a molecule of 5PAA instead 5PAED. We then obtained the structure of a hPGI-5PAA complex at 1.95 Å resolution. The final hPGI-5PAA model contains 4 chains of residues 1–556, 4 molecules of 5PAA, 4 molecules of polyethylene glycol, 2 molecules of glycerol and 1469 water molecules with a R/Rfree of 17/22%. Molecular structures, figures and scheme were generated with Pymol 2.0.5, Gimp 2.6.6, Chemdraw Pro 12.0 (Perkin-Elmer Informatics Inc., Cambridge, MA, USA) and Powerpoint softwares. Crystallographic data collection and refinement statistics of hPGI-5PAED complex are given in Table 2.

Accession numbers

Coordinates and structure factors have been deposited in the Protein Data Bank for hPGI-5PAED (**5j**) and hPGI-5PAA (**2**) complexes with accession number 6XUH and 6XUI, respectively.

Declaration of Competing Interest

The authors declare that they have no known competing financial interests or personal relationships that could have appeared to influence the work reported in this paper.

Acknowledgements

LA conducted this work in fulfilment of the requirements for a Ph.D. from the University of Paris-Saclay. One of the team (ECBB) is a member of the Laboratory of Excellence in Research on Medication and Innovative Therapeutics (LERMIT) supported by a grant from the Agence Nationale de la Recherche (ANR-10-LABX-33). This work received support from the French Infrastructure for Structural Biology (FRISBI ANR-10-INSB-0501). We thank the staff of the Proxima1 and Proxima2 beamlines at the SOLEIL synchrotron for assistance during the diffraction data collections. Jean-Pierre Baltaze (ICMMO) is gratefully acknowledged for his valuable help in NMR spectroscopy.

Appendix A. Supplementary material

Supplementary data to this article can be found online at https://doi.org/10.1016/j.bioorg.2020.104048.

References

[1] M. Salas, Spontaneaous and enzymatically catalysed anomerization of glucose 6-phosphate and anomeric specificity of related enzymes, J. Biol. Chem. 240 (1965) 561–568 http://www.jbc.org/content/240/2/561.
[2] K.J. Schray, S.J. Benkovic, P.A. Benkovic, I.A. Rose, Catalytic reactions of phosphoglucose isomerase with cyclic forms of glucose 6-phosphate and fructose 6-phosphate, J. Biol. Chem. 248 (1973) 2219–2224 http://www.jbc.org/content/248/6/2219.
[3] R. Hardré, C. Bonnette, L. Salmon, A. Gaudemer, Synthesis and evaluation of a new inhibitor of phosphoglucose isomerase: the enediolate analogue 5-phospho-D-arabinohydroxamate, Bioorg. Med. Chem. Lett. 8 (1998) 3435–3438, https://doi.org/10.1016/s0960-894x(98)00621-0.
[4] J.M. Chirgwin, E.A. Noltmann, The enediolate analogue 5-phosphoarabinonate as a mechanistic probe for phosphoglucose isomerase, J. Biol. Chem. 250 (1975) 7272–7276 http://www.jbc.org/content/250/18/7272.
[5] J. Read, J. Pearce, X. Li, H. Muirhead, J. Chirgwin, C. Davies, The crystal structure of human phosphoglucose isomerase at 1.6 A resolution: implications for catalytic mechanism, cytokine activity and haemolytic anaemia, J. Mol. Biol. 309 (2001) 447–463, https://doi.org/10.1006/jmbi.2001.4680.
[6] D. Arsenieva, C.J. Jeffery, Conformational changes in phosphoglucose isomerase induced by ligand binding, J. Mol. Biol. 323 (2002) 77–84, https://doi.org/10.1016/S0022-2836(02)00892-6.
[7] J.H. Lee, K.Z. Chang, V. Patel, C.J. Jeffery, Crystal structure of rabbit phosphoglucose isomerase complexed with its substrate D-fructose 6-phosphate, Biochemistry 40 (2001) 7799–7805, https://doi.org/10.1021/bi002916o.
[8] D. Arsenieva, R. Hardre, L. Salmon, C.J. Jeffery, The crystal structure of rabbit phosphoglucose isomerase complexed with 5-phospho-D-arabinonohydroxamic acid, Proc. Natl. Acad. Sci. USA 99 (2002) 5872–5877, https://doi.org/10.1073/pnas.052131799.
[9] C.J. Jeffery, R. Hardré, L. Salmon, Crystal structure of rabbit phosphoglucose isomerase complexed with 5-phospho-D-arabinonate identifies the role of Glu357 in catalysis, Biochemistry 40 (2001) 1560–1566 https://doi-org.proxy.scd.u-psud.fr/10.1021/bi0018483.
[10] C. Davies, H. Muirhead, J. Chirgwin, The structure of human phosphoglucose isomerase complexed with a transition-state analogue, Acta Crystallogr. D Biol. Crystallogr. 59 (2003) 1111–1113, https://doi.org/10.1107/s0907444903007352.

[11] J.H. Lee, C.J. Jeffery, The crystal structure of rabbit phosphoglucose isomerase complexed with D-sorbitol-6-phosphate, an analog of the open chain form of D-glucose-6-phosphate, Protein Sci. 14 (2005) 727–734, https://doi.org/10.1110/ps.041070205.
[12] C.J. Jeffery, Moonlighting proteins, Trends Biochem. Sci. 24 (1999) 8–11, https://doi.org/10.1016/S0968-0004(98)01335-8.
[13] P. Faik, J.I.H. Walker, A.A.M. Redmill, M.J. Morgan, Mouse glucose-6-phosphate isomerase and neuroleukin have identical 3′ sequences, Nature 332 (1988) 455–456, https://doi.org/10.1038/332455a0.
[14] M. Chaput, V. Claes, D. Portetelle, I. Cludts, A. Cravador, A. Burny, H. Gras, A. Tartar, The neurotrophic factor neuroleukin is 90% homologous with phosphohexose isomerase, Nature 332 (1988) 454–455, https://doi.org/10.1038/332454a0.
[15] W. Xu, K. Seiter, E. Feldman, T. Ahmed, J.W. Chiao, The differentiation and maturation mediator for human myeloid leukemia cells shares homology with neuroleukin or phosphoglucose isomerase, Blood 87 (1996) 4502–4506, https://doi.org/10.1182/blood.V87.11.4502.bloodjournal87114502.
[16] I. Matsumoto, A. Staub, C. Benoist, D. Mathis, Arthritis provoked by linked T and B cell recognition of a glycolytic enzyme, Science 286 (1999) 1732–1735, https://doi.org/10.1126/science.286.5445.1732.
[17] E. Yakirevich, Y. Naot, Cloning of a glucose phosphate isomerase/neuroleukin-like sperm antigen involved in sperm agglutination, Biol. Reproduction. 62 (2000) 1016–1023, https://doi.org/10.1095/biolreprod62.4.1016.
[18] M.-J. Cao, K. Osatomi, R. Matsuda, M. Ohkubo, K. Hara, T. Ishihara, Purification of a novel serine proteinase inhibitor from the skeletal muscle of white croaker (Argyrosomus argentatus), Biochem. Biophys. Res. Commun. 272 (2000) 485–489, https://doi.org/10.1006/bbrc.2000.2803.
[19] L.A. Liotta, R. Mandler, G. Murano, D.A. Katz, R.K. Gordon, P.K. Chiang, E. Schiffmann, Tumor cell autocrine motility factor, Proc. Natl. Acad. Sci. USA 83 (1986) 3302–3306, https://doi.org/10.1073/pnas.83.10.3302.
[20] H. Watanabe, K. Takehana, M. Date, T. Shinozaki, A. Raz, Tumor cell autocrine motility factor is the neuroleukin/phosphohexose isomerase polypeptide, Cancer Res. 56 (1996) 2960–2963 https://cancerres.aacrjournals.org/content/56/13/2960.
[21] H. Watanabe, P. Carmi, V. Hogan, T. Raz, S. Silletti, I.R. Nabi, A. Raz, Purification of human tumor cell autocrine motility factor and molecular cloning of its receptor, J. Biol. Chem. 266 (1991) 13442–13448 http://www.jbc.org/content/266/20/13442.
[22] O. Bodansky, Serum phosphohexose isomerase in cancer. II. as an index of tumor growth in metastatic carcinoma of the breast, Cancer 7 (1954) 1200–1226. https://doi.org/10.1002/1097-0142(195411)7:6%3C1200::AID-CNCR2820070612%3E3.0.CO;2-9.
[23] M.K. Schwartz, M.D. Greenberg, O. Bodansky, Comparative values of phosphatases and other serum enzymes in following patients with prostatic carcinoma, Cancer 16 (1963) 583–594, https://doi.org/10.1002/1097-0142(196305)16:5%3C583::AID-CNCR2820160507%3E3.0.CO;2-L.
[24] R. Guirguis, E. Schiffmann, B. Liu, D. Birkbeck, J. Engel, L. Liotta, Detection of autocrine motility factor in urine as a marker of bladder cancer, J. Natl. Cancer Inst. 80 (1988) 1203–1211, https://doi.org/10.1093/jnci/80.15.1203.
[25] M. Baumann, A. Kappl, T. Lang, K. Brand, W. Siegfried, E. Paterok, The diagnostic validity of the serum tumor marker phosphohexose isomerase (PHI) in patients with gastrointestinal, kidney, and breast cancer, Cancer Invest. 8 (1990) 351–356, https://doi.org/10.3109/07357909009012053.
[26] X. Filella, R. Molina, J. Jo, E. Mas, A.M. Ballesta, Serum phosphohexose isomerase activities in patients with colorectal cancer, Tumour Biol. 12 (1991) 360–367, https://doi.org/10.1159/000217737.
[27] N. Tanaka, A. Haga, H. Uemura, H. Akiyama, T. Funasaka, H. Nagase, A. Raz, K.T. Nakamura, Inhibition mechanism of cytokine activity of human autocrine motility factor examined by crystal structure analyses and site-directed mutagenesis studies, J. Mol. Biol. 318 (2002) 985–997, https://doi.org/10.1016/S0022-2836(02)00186-9.
[28] S. Tsutsumi, T. Yanagawa, T. Shimura, H. Kuwano, A. Raz, Autocrine motility factor signaling enhances pancreatic cancer metastasis, Clin. Cancer Res. 10 (2004) 7775–7784, https://doi.org/10.1158/1078-0432.CCR-04-1015.
[29] M. Devillers, L. Ahmad, H. Korri-Youssoufi, L. Salmon, Carbohydrate-based electrochemical biosensor for detection of a cancer biomarker in human plasma, Biosens. Bioelectron. 96 (2017) 178–185, https://doi.org/10.1016/j.bios.2017.04.031.
[30] L. Ahmad, L. Salmon, H. Korri-Youssoufi, Electrochemical detection of the human cancer biomarker 'autocrine motility factor-phosphoglucose isomerase' based on a biosensor formed with a monosaccharidic inhibitor, Sens. Actuators B Chem. 126933 (2019), https://doi.org/10.1016/j.snb.2019.126933.
[31] L. Ahmad, S. Plancqueel, V. Dubosclard, N. Lazar, W. Ghattas, I. Li de la Sierra-Gallay, H. van Tilbeurgh, L. Salmon, Crystal structure of phosphomannose isomerase from Candida albicans complexed with 5-phospho-d-arabinonhydrazide, FEBS Lett. 592 (2018) 1667–1680, https://doi.org/10.1002/1873-3468.13059.
[32] C. Roux, J.H. Lee, C.J. Jeffery, L. Salmon, Inhibition of type I and type II phosphomannose isomerases by the reaction intermediate analogue 5-phospho-D-arabinonohydroxamic acid supports a catalytic role for the metal cofactor, Biochemistry 43 (2004) 2926–2934, https://doi.org/10.1021/bi035688h.
[33] R. Hardré, L. Salmon, Competitive inhibitors of yeast phosphoglucose isomerase: synthesis and evaluation of new types of phosphorylated sugars from the synthon D-arabinonolactone-5-phosphate, Carbohydr. Res. 318 (1999) 110–115 https://doi-org.proxy.scd.u-psud.fr/10.1016/S0008-6215(99)00100-7.
[34] R.W. Gracy, E.A. Noltman, Studies on phosphomannose isomerase I. Isolation, homogeneity measurements, and determination of some physical properties, J. Biol. Chem. 243 (1968) 3161–3168.
[35] C. Roux, F. Bhatt, J. Foret, B. de Courcy, N. Gresh, J.-P. Piquemal, C.J. Jeffery, L. Salmon, The reaction mechanism of type I phosphomannose isomerases: New information from inhibition and polarizable molecular mechanics studies, Proteins. 79 (2011) 203–220, https://doi.org/10.1002/prot.22873.
[36] A.R. Bernard, T.N.C. Wells, A. Cleasby, F. Borlat, M.A. Payton, A.E.I. Proudfoot, Selenomethionine labelling of phosphomannose isomerase changes its kinetic properties, Eur. J. Biochem. 230 (1995) 111–118, https://doi.org/10.1111/j.1432-1033.1995.0111i.x.
[37] R.W. Gracy, B.E. Tilley, [84] Phosphoglucose isomerase of human erythrocytes and cardiac tissue, Methods Enzymol. (1975) 392–400, https://doi.org/10.1016/S0076-6879(75)41086-2.
[38] J.P. Gallivan, D.A. Dougherty, Cation-π interactions in structural biology, Proc. Natl. Acad. Sci. USA 96 (1999) 9459–9464 https://dx.doi.org/10.1073%2Fpnas.96.17.9459.
[39] A.S. Mahadevi, G.N. Sastry, Cation−π Interaction: Its role and relevance in chemistry, biology, and material science, Chem. Rev. 113 (2013) 2100–2138, https://doi.org/10.1021/cr300222d.
[40] A. Achari, S.E. Marshall, H. Muirhead, R.H. Palmier, E.A. Noltman, Glucose-6-phosphate isomerase, Phil. Trans. R. Soc. Lond. B. 293 (1981) 145–157, https://doi.org/10.1098/rstb.1981.0068.
[41] W. Kabsch, XDS, Acta Crystallogr. D Biol. Crystallogr. 66 (2010) 125–132. https://doi.org/10.1107/S0907444909047337.
[42] A.J. McCoy, R.W. Grosse-Kunstleve, P.D. Adams, M.D. Winn, L.C. Storoni, R.J. Read, Phaser crystallographic software, J Appl Crystallogr. 40 (2007) 658–674, https://doi.org/10.1107/S0021889807021206.
[43] K. Cowtan, The Buccaneer software for automated model building. 1. Tracing protein chains, Acta Cryst D. 62 (2006) 1002–1011, https://doi.org/10.1107/S0907444906022116.
[44] P. Emsley, K. Cowtan, Coot: model-building tools for molecular graphics, Acta Crystallogr. D Biol. Crystallogr. 60 (2004) 2126–2132, https://doi.org/10.1107/S0907444904019158.
[45] G.N. Murshudov, P. Skubák, A.A. Lebedev, N.S. Pannu, R.A. Steiner, R.A. Nicholls, M.D. Winn, F. Long, A.A. Vagin, REFMAC5 for the refinement of macromolecular crystal structures, Acta Crystallogr. D Biol. Crystallogr. 67 (2011) 355–367, https://doi.org/10.1107/S0907444911001314.